Violet Bioluminescence and Fast Kinetics from W92F Obelin: Structure-Based Proposals for the Bioluminescence Triggering and the Identification of the Emitting Species†

Eugene S. Vysotski,‡,§ Zhi-Jie Liu,‡ Svetlana V. Markova,‡,§ John R. Blinks,|| Lu Deng,⊥ Ludmila A. Frank,§ Michelle Herko,|| Natalia P. Malikova,§ John P. Rose,‡ Bi−Cheng Wang,‡ and John Lee*,‡

Department of Biochemistry and Molecular Biology and Department of Chemistry, University of Georgia, Athens, Georgia, Photobiology Lab, Institute of Biophysics RAS, SB, Krasnoyarsk, Russia, and Friday Harbor Labs, University of Washington, Seattle, Washington

Received December 2, 2002; Revised Manuscript Received March 27, 2003

ABSTRACT: Obelin from the hydroid *Obelia longissima* and aequorin are members of a subfamily of Ca^{2+}-regulated photoproteins that is a part of the larger EF-hand calcium binding protein family. On the addition of Ca^{2+}, obelin generates a blue bioluminescence emission ($\lambda_{max} = 485$ nm) as the result of the oxidative decarboxylation of the bound substrate, coelenterazine. The W92F obelin mutant is noteworthy because of the unusually high speed with which it responds to sudden changes of [Ca^{2+}] and because it emits violet light rather than blue due to a prominent band with $\lambda_{max} = 405$ nm. Increase of pH in the range from 5.5 to 8.5 and using D_2O both diminish the contribution of the 405 nm band, indicating that excited state proton transfer is involved. Fluorescence model studies have suggested the origin of the 485 nm emission as the excited state of an anion of coelenteramide, the bioluminescence reaction product, and 405 nm from the excited neutral state. Assuming that the dimensions of the substrate binding cavity do not change during the excited state formation, a His22 residue within hydrogen bonding distance to the 6-(p-hydroxy)-phenyl group of the excited coelenteramide is a likely candidate for accepting the phenol proton to produce an ion-pair excited state, in support of recent suggestions for the bioluminescence emitting state. The proton transfer could be impeded by removal of the Trp92 H-bond, resulting in strong enhancement of a 405 nm band giving the violet color of bioluminescence. Comparative analysis of 3D structures of the wild-type (WT) and W92F obelins reveals that there are structural displacements of certain key Ca^{2+}-ligating residues in the loops of the two C-terminal EF hands as well as clear differences in hydrogen bond networks in W92F. For instance, the hydrogen bond between the side-chain oxygen atom of Asp169 and the main-chain nitrogen of Arg112 binds together the incoming α-helix of loop III and the exiting α-helix of loop IV in WT, providing probably concerted changes in these EF hands on calcium binding. But this linkage is not found in W92F obelin. These differences apparently do not change the overall affinity to calcium of W92F obelin but may account for the kinetic differences between the WT and mutant obelins. From analysis of the hydrogen bond network in the coelenterazine binding cavity, it is proposed that the trigger for bioluminescence reaction in these Ca^{2+}-regulated photoproteins may be a shift of the hydrogen bond donor−acceptor separations around the coelenterazine-2-hydroperoxy substrate, initiated by small spatial adjustment of the exiting α-helix of loop IV.

Obelin is a 22-kDa calcium-regulated photoprotein found in bioluminescent marine hydroids, and the cDNA[1] for the recombinant obelin used in this study was isolated from *Obelia longissima* (*1*, *2*). Obelin is a member of a family of Ca^{2+}-regulated photoproteins that are responsible for bioluminescence of certain marine organisms, mostly coelenterates (*3*). Aequorin, named for its origin in the jellyfish *Aequorea*, has been known as requiring Ca^{2+} for the regulation of its bioluminescence function since its discovery in the early 60's (*4*). The primary sequence determined much later revealed canonical Ca^{2+}-binding EF hands, and this is now known to be standard in the sequences of calcium-regulated photoproteins from other genera, all of which exhibit high homology to aequorin (*2*, *5*, *6*). The EF-hand calcium binding

† This work was supported by ONR Grant N 00014-99-1-0414, Georgia Research Alliance, by Grant 02-04-49419 from the Fundamental Research Foundation of the Russian Academy of Sciences, and by Grant #NA76RG0119, Project R/B-32 from the National Oceanic and Atmospheric Administration to Washington Sea Grant Program, University of Washington. The views expressed herein are those of the authors and do not necessarily reflect the views of NOAA or any of its subagencies.

* Corresponding author. E-mail: John Lee jlee@arches.uga.edu. Tel: 706/542-1764. Fax: 706/542-1738.

‡ Department of Biochemistry and Molecular Biology, University of Georgia.

§ Institute of Biophysics RAS.

|| University of Washington.

⊥ Department of Chemistry, University of Georgia.

[1] Abbreviations: HTH, helix−turn−helix; IPTG, isopropyl β-D-thiogalactopyranoside; DTT, DL-dithiothreitol; EDTA, ethylenediaminetetraacetic acid; EGTA, ethylene glycol-OO′-bis(2aminoethyl)-*N*,*N*,*N*′-*N*′-tetraacetic acid; cDNA, complementary DNA; WT, wild-type; CIL, Ca^{2+}-independent luminescence.

10.1021/bi027258h CCC: $25.00
Published on Web 05/03/2003

Scheme 1

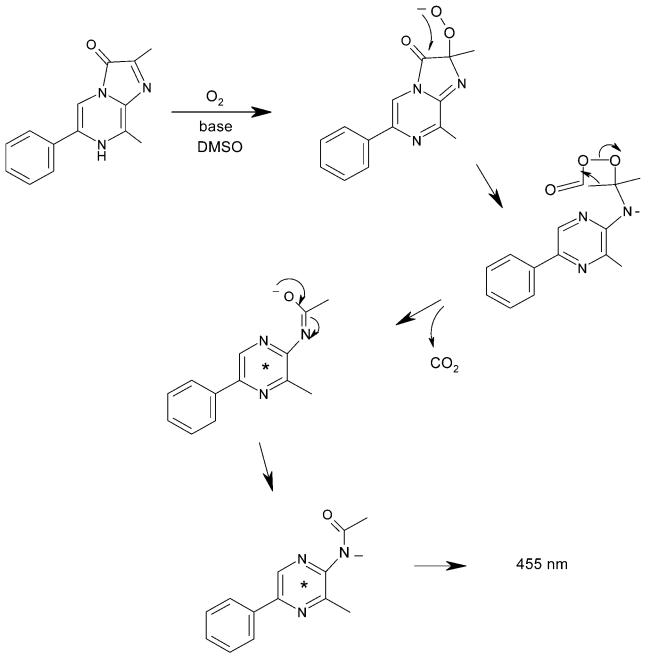

protein family (*7*) is one of the most extensively studied protein families (*8*). However, the distinguishing feature of the photoproteins is that the addition of Ca^{2+} causes the emission of a blue bioluminescence and the formation of a fluorescent protein-bound product.

The bioluminescence activity of these photoproteins depends on the presence of a tightly but noncovalently bound imidazolopyrazine derivative appropriately called "coelenterazine". Early in the history of this subject, McCapra and Chang (*9*) investigated the chemiluminescence of an imidazolopyrazine derivative analogous to coelenterazine and established the reaction mechanism in Scheme 1. They proposed this mechanism as a model for the bioluminescence systems that utilize structurally related substrates, namely, the luciferin of the ostracod *Vargula* (*Cypridina*) and coelenterazine in the photoprotein aequorin. Subsequent biochemical and structural investigations have convincingly verified this proposal.

Two features of the calcium-regulated photoproteins distinguish them from the luciferin−luciferase bioluminescence systems that operate by this same chemical mechanism but have classical enzyme−substrate kinetics. The first is that the bioluminescence kinetics of photoproteins is not influenced by oxygen concentration (*4*, *10*). It was suggested, therefore, that in aequorin the coelenterazine was bound within the photoprotein as the stabilized peroxy−coelenterazine intermediate (*11*), and this proposal has been confirmed in a recent structural study (*12*). The second feature is that although calcium is not essential for the luminescence (photoproteins alone give off a very low level of light emission called the "calcium-independent luminescence"), the light intensity is increased up to 1 million-fold or more on the addition of calcium. It is supposed, therefore, that the binding of Ca^{2+} induces some conformational change in the photoprotein which destabilizes the peroxycoelenterazine (Scheme 2) and allows it, according to the model of Scheme 1, to decompose to the excited state of the protein bound coelenteramide, which is followed by the emission of the blue bioluminescence (λ_{max} = 465 nm for aequorin).

Scheme 2

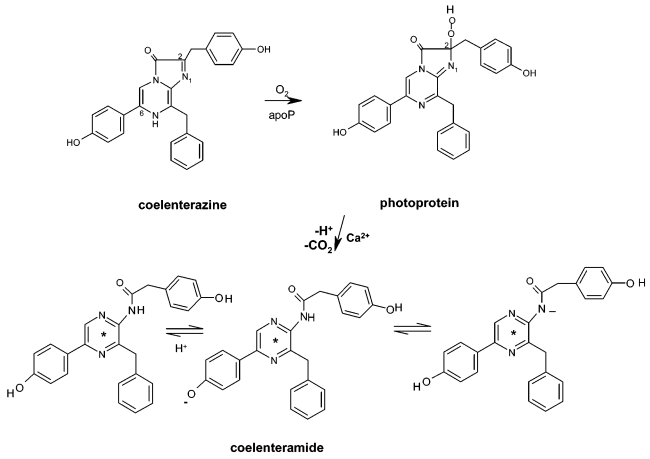

The crystal structures of two photoproteins are now known: aequorin and obelin (*12*, *13*). In fact, the spatial structure of obelin has now been determined to atomic resolution (<1.1 Å), the highest of any EF-hand protein (*14*, *15*). As expected from the homology of their primary sequences, aequorin and obelin have the same basic tertiary structure—a compact globule containing four HTH units, three of which are classical EF hands. It is supposed that only the N-terminal loop I and the C-terminal loops III and IV bind Ca^{2+} because the second N-terminal loop II does not have the canonical sequence for Ca^{2+} binding (*13*). The peroxy−coelenterazine is buried in a highly hydrophobic cavity located in corresponding positions in the two proteins. The peroxide substitution on the coelenterazine (Scheme 2) was suggested in the aequorin structure, where weak electron density consistent with the presence of two oxygens was found at the C2-position of the coelenterazine, in accordance with the prediction from the many earlier biochemical and chemical model studies (*11*). A puzzle, however, was that in *O. longissima* obelin only one oxygen could be observed in the 1.7 Å structure first reported (*13*). A new atomic resolution (1.0 Å) structure now reveals very weak electron density at the second oxygen (O34) position (*15*).

The Ca^{2+}-regulated photoproteins are distinctive also in having a primary sequence with many tryptophan, cysteine, and histidine residues (obelin from *O. longissima* contains six tryptophan, five cysteine, and five histidine residues, for example), which are not commonly found in calcium-binding proteins (*7*, *16*). Four tryptophans (Trp92, 114, 135, 179) and two histidines (His22, 175) are located in the coelenterazine-oxygen binding pocket (*13*). Any of these might be involved in the oxidation of coelenterazine or in the formation of the excited state. Ohmiya et al. (*17*) made all the Trp to Phe mutants of aequorin and found that one of them, W86F, together with the usual bioluminescence emission with λ_{max}= 465 nm, showed an additional band with λ_{max}= 400 nm. According to solution fluorescence studies of coelenteramide and its analogues, the bioluminescence bands at 465 and 400 nm originate from the singlet electronic excited states of the amide monoanion and neutral species (Scheme 2), respectively (*18*). Recently, in an attempt to understand why the substitution of this one amino acid favors the formation of the neutral species of the excited state of coelenteramide, we produced the obelin mutant, W92F, and determined its spatial structure (*19*). Trp92 in

obelin corresponds to the Trp86 in aequorin, and in both proteins these tryptophans are proximate to the bound coelenterazine (*12*, *13*). The bioluminescence of W92F obelin is a violet color as a result of the addition of a new band with $\lambda_{max} = 405$ nm and an intensity similar to that of the band at the longer wavelength. The substitution of Trp92 in obelin results in a larger relative intensity of the shorter wavelength emission than in case of aequorin. The crystal structure of the W92F obelin, solved at 1.72 Å resolution, revealed no significant differences between the dimensions of the active sites of WT and W92F obelins (*19*). It was proposed that the bioluminescence spectral shift arises from removal of a hydrogen bond from the indole of Trp92 close to the hydroxyl belonging to the 6-*p*-hydroxyphenyl group of the bound coelenterazine.

Photoproteins have found extensive applications as gene expression probes, as immunoassay tags, and as biological calcium indicators. For this last purpose, the speed with which the bioluminescence reflects rapid changes in $[Ca^{2+}]$ is a critical property. A thorough rapid-mixing study of photoprotein kinetics was carried out with aequorin (*20*). The authors reported that the rate constant for the rise of light intensity was about 100 s^{-1} and independent of $[Ca^{2+}]$. This can be too slow to follow rapid intracellular Ca^{2+} transients without distortion, and it would be useful to have faster responding photoproteins.

In this paper we report a continuation of our studies of W92F obelin. We compare a number of properties of this mutant with the corresponding ones of WT obelin: spatial structure, spectra, stopped-flow kinetics, sensitivity to calcium, and some effects of Mg^{2+}. Of particular note is that W92F obelin responds more rapidly to sudden changes in $[Ca^{2+}]$ than any other photoprotein so far described. From details of the three-dimensional structure, we propose a mechanism for the trigger of the coelenterazine decarboxylation and for the formation of different ionic excited states of the product coelenteramide.

EXPERIMENTAL PROCEDURES

Reagents. The QuickChange site-directed mutagenesis kit, competent cells of *E. coli* strains XL1-Blue, and BL21-Gold, were from Stratagene (La Jolla, CA). Oligonucleotides were purchased from MWG-Biotech (High Point, NC). Restriction and modification enzymes were from Promega (Madison, WI). Coelenterazine was from Prolume Ltd. (Pittsburgh, PA). Chelex-100 chelating resin (100−200 mesh), BioGel P2 resin, Bio-Rad DC Protein Assay Kit, and the Bio-Scale DEAE 10 anion exchange column were from Bio-Rad (Richmond, CA). DEAE-Sepharose Fast Flow was from Amersham-Pharmacia-Biotech (Piscataway, NJ). EGTA was from Fluka (batch number 276355/1 1291). D_2O was purchased from Cambridge Isotope Laboratories (Andover, MA). All other chemicals were from standard laboratory supply houses, and were reagent grade or better.

Site-Directed Mutagenesis, Growth of Bacterial Cultures, and Induction. Site-directed mutagenesis was carried out as described in (*19*) on the template pET19-OL8 *E. coli* expression plasmid carrying the cDNA for *O. longissima* WT apoobelin (*21*). We used the QuickChange site-directed mutagenesis kit according to the protocol supplied with the kit. Two mutagenic oligonucleotides containing the desired mutations—the sense primer 5′-CAATTCCTCGATGGAT-TCAAACAATTAGCG-3′ and antisense primer 5′-CGCCA-ATTGTTTGAATCCATCGAGGAATTG-3′—each complementary to opposite vector strands, were used to replicate the double-stranded plasmid template. The changed nucleotides causing the mutations are underlined. Plasmid harboring the mutation was verified by DNA sequence analysis (MWG-Biotech, High Point, NC) and introduced into *E. coli* strain BL21 (DE3)-Gold for expression of mutant protein. *E. coli* BL21(DE3)-Gold cells were grown in media containing 200 μg/mL ampicillin or 50 μg/mL carbenicillin. For protein production, the transformed *E. coli* BL21-Gold was cultivated with vigorous shaking at 37 °C in LB medium containing ampicillin and induced with 1 mM IPTG when the culture reached an OD_{600} of 0.5−0.6. After addition of IPTG, the cultivation was continued for 3 h.

Purification of W92F Obelin. The mutant was purified and charged with coelenterazine as previously reported for WT recombinant obelins (*21*−*23*). The final product was homogeneous according to LC-electrospray ionization mass spectrometry. The molecular weight of the W92F obelin (22,040 Da) determined with this method is in an excellent agreement with that calculated from the amino acid sequence excluding Met1 (22 040 Da), as was also observed for WT obelin (*24*). For investigation of coelenterazine binding kinetics, the apoWT and apoW92F were purified according to the procedure described in (*22*). The apoproteins (2×10^{-6} M) were charged with a 10-fold molar excess of coelenterazine in a 20 mM Tris-HCl buffer, pH 7.0, containing 5 mM EDTA and 10 mM DTT at 4 °C.

Ca^{2+}-Discharged W92F Obelin. A concentrated solution of W92F obelin (8−10 mg/mL) was diluted 10 times with 50 mM Bis-Tris propane buffer, pH 7.0, and a concentrated solution of $CaCl_2$ (final concentration of calcium in the sample = 1 mM) was added. When the bioluminescence reaction had ceased, the protein sample was concentrated using Amicon Centricon-10 tubes and passed through a BioGel P2 column equilibrated with 50 mM Bis-Tris propane buffer, pH 5.5, 7.0, or 8.5, with 1 mM $CaCl_2$ or 1 mM EDTA. These Ca^{2+}-discharged W92F obelin samples were then concentrated with Amicon Centricon-10 tubes.

Crystallization, Data Collection, and Refinement. The preparation of W92F obelin crystals and their properties were previously described (*19*). Crystals exposed to calcium ion either before or after X-ray irradiation emit light, confirming that the crystals consist of an active photoprotein. The W92F obelin crystal was flash-cooled to 100 K and maintained at this temperature for measurement. The data for molecular replacement solution were collected to 2.5 Å resolution on a RAXIS IV image plate detector using MSC blue confocal optics focused Cu Kα X-rays generated on a Rigaku RU200 rotating anode running at 5.0 kw. The 1.72 Å resolution data were collected later using the same crystal at beamline ID-17 (IMCA-CAT), Advanced Photon Source (APS), Argonne National Laboratory, using a MarResearch 165 mm CCD detector and 0.94 Å X-rays. Data processing was carried out using HKL2000 (*25*). The crystal belongs to P41212 space group, and there is only one molecule in the asymmetric unit. CNS 1.0 was used to perform the molecular replacement method using obelin (PDB entry 1EL4) as a search model. The initial model, oriented and positioned according to the molecular replacement solution, was examined by the

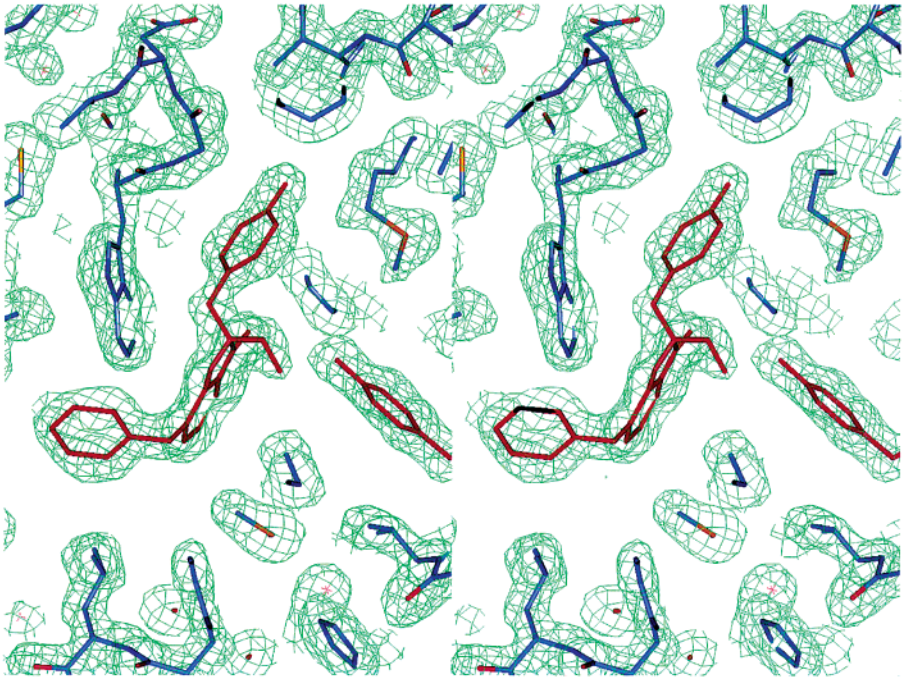

FIGURE 1: Stereo diagram of the 2Fo-Fc composite omit map at 1.72 Å covering the final model of the peroxycoelenterazine (orange) in the active site of W92F obelin.

Table 1: X-Ray Crystallography Data Statistics

(a) Data Collection and Processing Statistics	
data set used for phasing	
wavelength (Å)	1.54
resolution[a] (Å)	2.5
completeness (%)	99.9
Bijvoet redundancy	5.8
R_{merge}[b] (%)	3.7 (8.0)
data set used for refinement	
wavelength(Å)	0.94
resolution[a] (Å)	1.72
completeness (%)	93.7
R_{merge}[b] (%)	3.8 (21.6)
(b) Refinement Statistics	
R value $2\sigma_F$ cutoff	0.232
R value all data	0.213
free *R* value	0.242
free *R* value test set	1710 reflections
RMS deviations from ideality	
bond lengths(Å)	0.005
bond angles	1.1°
dihedral angles	18.9°
improper angles	0.69°
Wilson *B* value(Å^2)	25.6
mean *B* value(Å^2)	26.4
coordinate error(Å)[c]	0.21
resolution range(Å)	26.28−1.72
data cutoff	2.0 σ_F
number of reflections	21683 reflections
completeness for range	93.7%
number of protein atoms	1452
number of SUBSTRATE atoms	34
number of solvent atoms:	212

[a] Highest resolution of data set followed by resolution range in highest bin for compiling statistics. [b] $R_{merge} = \Sigma\Sigma_j|\mathbf{F} - \langle\mathbf{F}\rangle|/\Sigma\langle\mathbf{F}\rangle$. [c] Estimated coordinate error from the Luzatti plot (*29*).

program O (*26*) to inspect the crystal packing. A further search model was made by truncating the F92 side chain and deleting ten N-terminal residues because of the unfavorable contacts between symmetrically related molecules. The refinement was carried out with CNS 1.0 (*27*). The first step

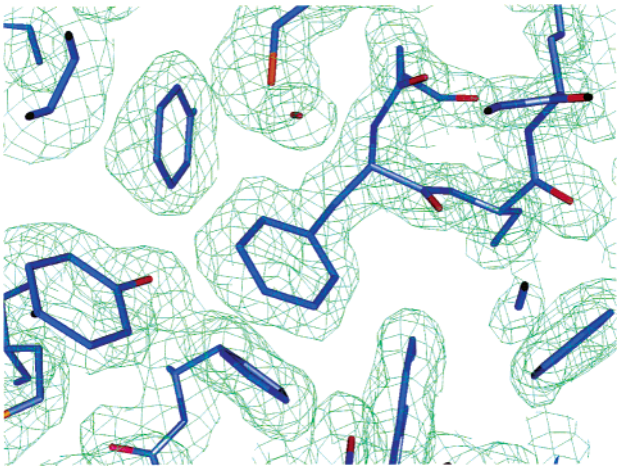

FIGURE 2: The F92 mutation fitted onto the 2Fo-Fc composite omit map at 1.72 Å.

was based on rigid-body refinement with the truncated model in the resolution range 20.0−3.0 Å. Several cycles of minimization and simulated-annealing refinement, followed by *B*-factor refinement and water pick-up, resulted in a final *R*-factor of 21.3% and free *R*-factor of 24.2% using 8% reflection data set for cross-validation analysis. The composite omit maps were used to assist in building the structure. During the course of the refinement, the side chains were adjusted stepwise, and the truncated side chains were rebuilt. The $F_o - F_c$ maps were calculated to aid the rebuilding of the truncated N-terminal. Residues from 1 to 4 were disordered. The quality of the model was checked using PROCHECK (*28*). All the results are summarized in Table 1. Figure 1 shows the superposition of the refined model around the active site in a $2F_o-F_c$ composite omit map. Figure 2 is the fitting of the Phe92 residue with the $2F_o-F_c$ composite omit map. The atomic coordinates are available with accession code 1JF2 in the Protein Data Bank.

Bioluminescence Assay and Spectral Measurements. The procedures for measurement of bioluminescence activity and corrected spectra were as detailed elsewhere (*23*). Calcium-independent luminescence was measured from undiluted concentrated photoprotein samples placed in the luminometer cell. The solution of the photoprotein also contained 5 mM EDTA or 2 mM EGTA. To measure the bioluminescence spectrum in D_2O, the W92F obelin sample at a protein concentration of 8.92 mg/mL in 1 mM EDTA, 10 mM K/Na phosphate buffer pH 7.0, was diluted 10-fold in D_2O containing 1 mM EDTA, 10 mM Tris-HCl, and concentrated with Amicon Centricon-10 tubes back to about 9 mg/mL. This procedure was repeated three times. A 10 mM Tris-HCl buffer in D_2O was prepared from 1 M Tris-HCl pH 7.0 stock solution by dilution with D_2O containing 1 mM EDTA. The pD was determined as pH + 0.4.

Ca^{2+} Concentration-Effect Curves and Rapid-mIxing Kinetic Measurements. These measurements were carried out with EDTA-free solutions of the photoprotein samples as previously described (*22*, *23*, *30*). Ca-EGTA buffers (2 mM total EGTA) were used to establish Ca^{2+} concentrations below about 10^{-5} M and simple dilutions of $CaCl_2$ for higher Ca^{2+} concentrations (*31*). When high concentrations of Ca^{2+} or Mg^{2+} were added, [KCl] was reduced to keep the ionic strength constant. When measurements were to be in solution containing Mg^{2+}, the photoprotein was preequilibrated with the same [Mg^{2+}]. This is important because Mg^{2+} ions bind to the photoprotein much more slowly than does Ca^{2+}, and the effects of Mg^{2+} are attenuated if preequilibration is not achieved (*32*). For the Ca^{2+} concentration-effect curves, peak light intensity was measured after 10 μL of photoprotein solution was forcefully injected into 1 mL of the test solution. Light intensity (L) measurements were converted to units of L/L_{int} by first determining L/L_{max} and then multiplying by the maximum peak-to-integral ratio (L_{max}/L_{int}) determined from stopped-flow measurements carried out under the same conditions and with the same sample of photoprotein. The fast kinetics of the light response after sudden exposure to a saturating Ca^{2+} concentration were examined with a stopped-flow machine modeled after that described by Gibson and Milnes (*33*), which provided a deadtime of about 1.5 ms. The Ca^{2+} syringe contained 40 mM Ca^{2+}, 30 mM KCl, 5 mM PIPES buffer, pH 7.0, so the final [Ca^{2+}] in the reaction mixture was 20 mM. The photoprotein was dissolved in a Ca^{2+}-free solution of the same ionic strength: 150 mM KCl, 5 mM PIPES, pH 7.0. The rise rate constant was calculated by one-exponential fit with SigmaPlot in the range from zero time to the time when the light signal reaches maximum (see Figure 5) with the equation: $L/L_{int} = (L/L_{int})_o + a \times (1 - e^{-k_{rise}t})$. Usually about 10 shots are averaged for the fitting and the stated error is the standard deviation of the fit. When Mg^{2+} was used, the same concentration was added to both syringes of the stopped-flow machine. When 10 mM Mg^{2+} was added, the KCl in the calcium solution was omitted in order to keep ionic strength constant.

RESULTS

Spectral Properties. The absorption spectrum of obelin is unchanged after the W92F mutation, except for an increase in A460/A280 resulting from the substitutionof one of the six Trp residues (*19*). A pH change over the range 5.5−8.5 has essentially no effect on the absorption spectrum of W92F obelin or on that of its product (λ_{max} = 347 nm) after the bioluminescence reaction. Removal of Ca^{2+} shifts the product λ_{max} to 334 nm. Figure 3 (left) shows, however, that pH has a clear influence on the bimodal bioluminescence emission spectrum from W92F obelin; acidification causes the relative contribution of the 467 nm band to decrease. The pH range that can be examined is of course limited by the stability of the photoprotein but measurements at intermediate pHs (not shown) suggest a midpoint for the change around pH 7. For WT obelin, a pH change over this same range has no effect on the bioluminescence spectrum (not shown). Substitution of H_2O by D_2O results in an increase in the relative contribution of this 467 nm band (Figure 3, right).

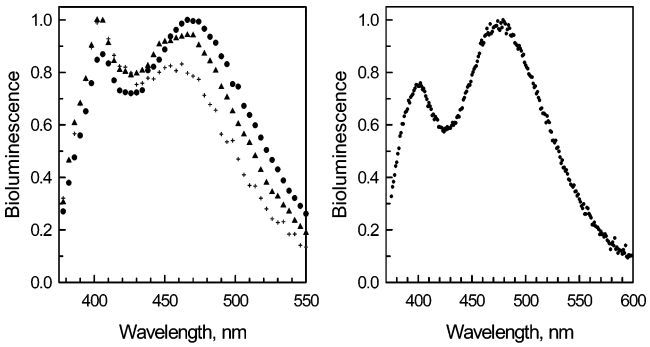

FIGURE 3: Bioluminescence spectra of W92F obelin on addition of Ca^{2+}. Left: pH 5.5 (+), 7.0 (▲), and 8.5 (●) in 50 mM Bis-Tris propane buffer. Right: in D_2O at pD 7.0 containing 10 mM Tris-HCl and 1 mM EDTA. All at room temperature.

The fluorescence of Ca^{2+}-discharged W92F obelin is green (λ_{max} = 510 nm, pH 7.0) and is very similar to that of Ca^{2+}-discharged WT obelin (*23*). At either pH 8.5 or 5.5, the fluorescence maximum shifts to around 500 nm, and there are also further small shifts due to the presence or absence of Ca^{2+}. As with the absorption spectra, there is no pH effect on the excitation maxima but again, these maxima shift to shorter wavelengths on removal of Ca^{2+}. The fluorescence emission anisotropy measured over the long-wavelength excitation band (310−360 nm) is approximately constant in the range 0.30−0.36, the value also having a small dependence on the pH or removal of Ca^{2+}. This high anisotropy indicates that the fluorophore is rigidly bound to the protein.

Kinetics of apoW92F Charging with Coelenterazine, Thermal Stability, and Other Properties of W92F Obelin. The apophotoprotein can be converted to the bioluminescent active photoprotein by incubation with synthetic coelenterazine under Ca^{2+}-free conditions in the presence of oxygen and SH-reducing reagents. The mechanism of this charging reaction is not known, and some amino acid residues of protein are important for the process (*34*, *35*). The kinetics of charging apoW92F are the same as for apoWT, implying that Trp92 does not participate directly in this reaction (data not shown).

The specific bioluminescence activity and the Ca^{2+}-independent luminescence are also practically the same for both photoproteins. There is some difference in thermal stability—the WT obelin is slightly more stable than W92F obelin in the temperature range 4−40 °C. For instance, the inactivation rate constants calculated by fitting inactivation curves measured at 40 °C to single exponentials are 1.5×10^{-2} and 1.8×10^{-2} min^{-1} for WT obelin and W92F obelin, respectively (data not shown).

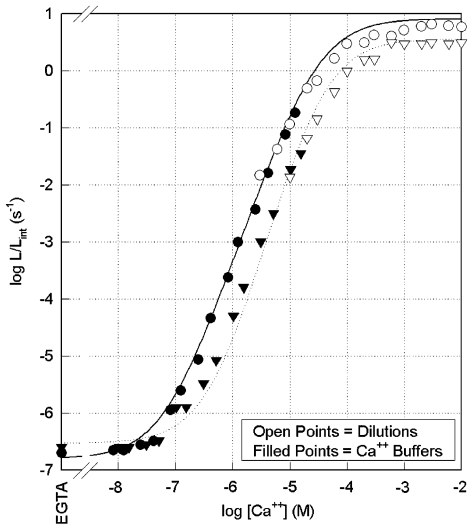

FIGURE 4: Ca^{2+} concentration-effect curves for W92F obelin without (circles) and with (triangles) 10 mM Mg^{2+}, pH 7.0, 20 °C. Both the mutant and WT (solid lines) show the same relationship with slope of 2.5 on the log−log scale and the same Mg^{2+} inhibition. Filled symbols, Ca-EGTA buffer; open symbols, dilutions of $CaCl_2$. L = light intensity; L_{int} = total light yield on reaction with excess Ca^{2+}.

Calcium Concentration-Effect Relation. The Ca^{2+} sensitivity of obelin is practically unchanged by the W92F mutation. Figure 4 shows Ca^{2+} concentration-effect curves for W92F obelin determined in the absence (circles) and presence (triangles) of 10 mM Mg^{2+}. Ca^{2+} concentration-effect curves for WT obelin under the same conditions are the lines (solid line, without Mg^{2+}; dashed line, with 10 mM Mg^{2+}). The curves are log−log plots in which light intensities have been expressed in terms of a ratio that we have termed the fractional rate of discharge (L/L_{int}). (In effect, light intensities are normalized to the total amount of light that the sample of photoprotein yields when discharged in saturating [Ca^{2+}]—for a detailed explanation see refs *22* and *23*). The curves for both proteins are sigmoid on a log−log plot, with maximum slopes of about 2.5. In both cases the vertical span is about 7.5 log units. The differences between the curves for W92F and WT obelin are slight, and most are probably within experimental error. One real difference is that peak light intensity in saturating [Ca^{2+}] is slightly lower for W92F obelin (log L/L_{int} = 6.5) than that for WT obelin (8.1). The level of the Ca^{2+} -independent luminescence (CIL) is not significantly changed by the W92F mutation, and the influence of 10 mM Mg^{2+} on the entire concentration effect curve is similar for the two proteins as well. An addition of 10 mM Mg^{2+} increased the calcium-independent luminescence of both proteins slightly but consistently. This was checked in each experiment by noting the effect on the CIL of adding Mg^{2+} to a cuvette already containing the photoprotein and 2 mM EGTA.

Rapid Mixing Stopped-Flow Kinetics. On a slow time scale, the kinetic pattern of the light emission obtained after rapid mixing of Ca^{2+} with W92F is very similar to that recorded with WT obelin (see Figure 8 of ref *22*). In both WT obelin and the W92F mutant, 10 mM Mg^{2+} reduces the maximum light emission by about 50%. The decay of the light emission is slowed enough so that the total amount of light emitted in the flash is essentially unchanged.

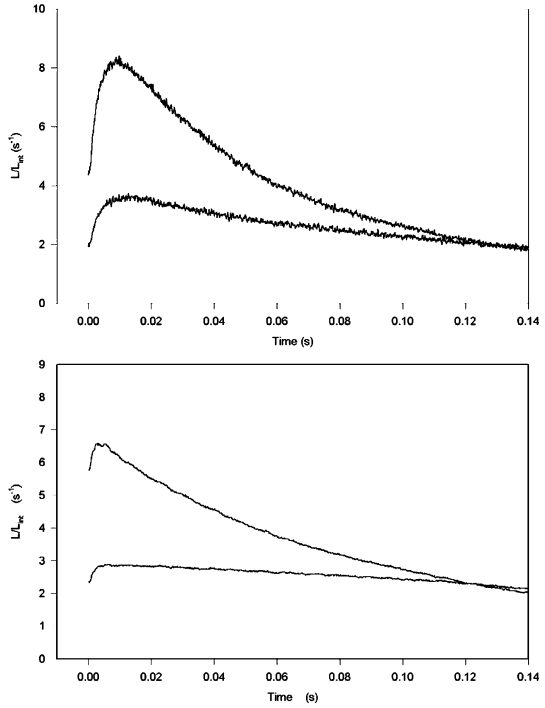

FIGURE 5: Stopped-flow bioluminescence intensity from 20 mM Ca^{2+} addition to (top panel) WT obelin and (lower panel) W92F obelin. The top curve is without Mg^{2+}, the lower with 10 mM (20 °C). The curves are individual shots (no signal averaging).

The rate of rise of light intensity after rapid mixing with Ca^{2+} is what limits the ability of the light signal to follow rapid changes in [Ca^{2+}]. In this respect a dramatic difference between WT and W92F obelin is observed (Figure 5). The time to peak light emission is considerably reduced in the mutant (Figure 5, lower panel), and the rate of rise of luminescence is correspondingly higher.

It is immediately obvious that the rate of rise of luminescence must be greatly increased in the W92F mutant because a substantially higher level of light emission is reached by the time that flow stops (i.e., during the dead time). By fitting a single exponential to the rising phase of each light signal, we estimate that in the absence of Mg^{2+} the rate constant for the rise of luminescence is increased from 405 ± 4 s^{-1} in WT obelin to 992 ± 37 s^{-1} in W92F obelin. The corresponding figures obtained in the presence of 10 mM Mg^{2+} were 352 ± 4 s^{-1} for WT obelin and 774 ± 14 s^{-1} for the mutant. It is also worth noting that the time to peak light intensity is not much prolonged by 10 mM Mg^{2+}, either for WT obelin or W92F. This stands in sharp contrast to the situation with aequorin and many other photoproteins (*22*).

Overall Structure of W92F Obelin. W92F obelin has a highly compact, globular structure with high helix content (Figure 6A) and closely resembles WT obelin (Figure 6B). The final model includes 190 of the 195 amino acids (1521 atoms), one peroxy−coelenterazine molecule (34 atoms) and 128 solvent molecules. The Cα atomic positions of W92F obelin versus WT obelin have an average rms deviation of around 0.5 Å (Figure 7A) (10 residues of the N-terminal are not counted because of their randomness caused by exposure to solvent). Although the overall structural features of WT obelin are well conserved in W92F obelin, there are regions where deviation of the Cα atoms is high.

One is within the loop of HTH motif III, Lys124-Ser127 (Figure 7) where the main-chain rms deviation is in the range

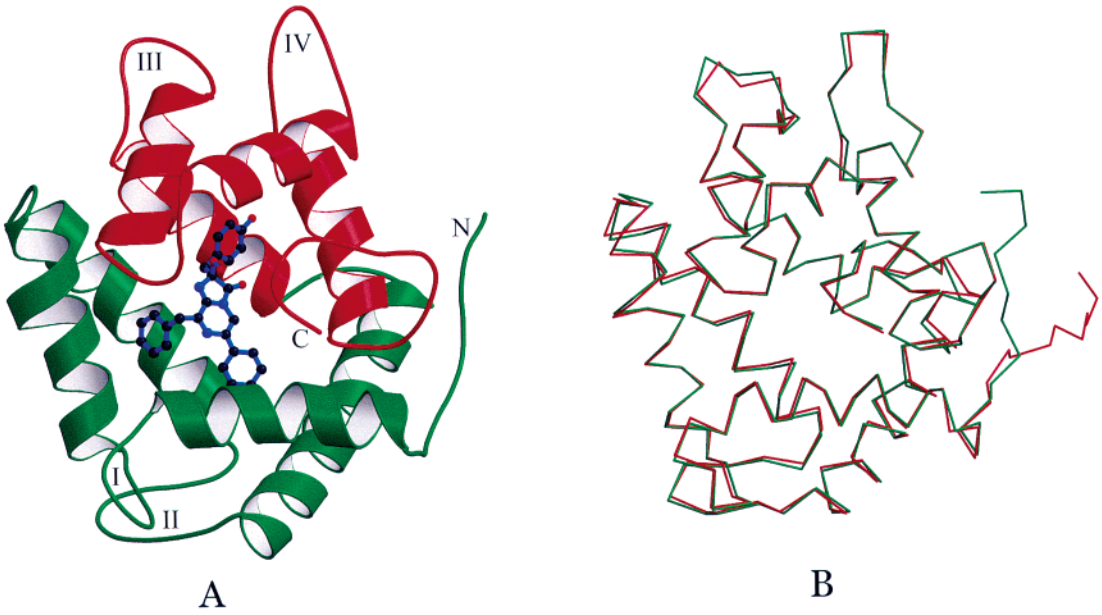

FIGURE 6: (A) The ribbon diagram of W92F obelin. The overall fold is characterized by two domains, N-terminal domain (green) and C-terminal domain (red). Each domain contains one pair of helix-turn-helix motifs, forming an almost entirely helical, highly compact and globular molecule. The expected calcium binding sites are the loops of motifs I, III, and IV. Motif II is not functional for calcium binding. The peroxy−coelenterazine (blue) resides into a hydrophobic core cavity formed by residues from the four helix−turn−helix motifs. (B) The superposition of W92F mutant (green) and WT obelin (red).

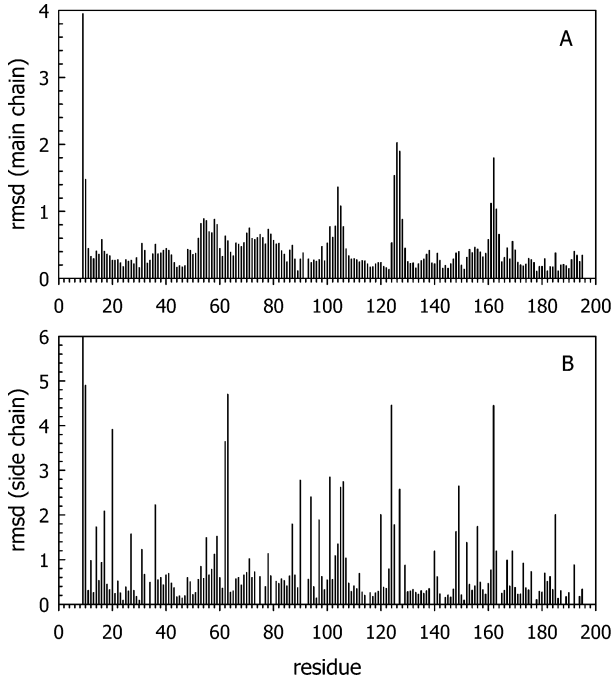

FIGURE 7: Root-mean-square deviation of Cα atoms (A) and side chain atoms (B) of the residue displacements (Å) between the obelin and its W92F mutant.

1.6−3.3 Å. Another includes Asp161−Ser163 residues in loop IV with rms deviation in the range 1.0−3.4 Å. Both these loops are putative Ca^{2+}-binding sites. It is possible that crystal packing is responsible for the difference observed in loop IV because in W92F there is an intermolecular hydrogen bond observed (Asn162 OD1 to Arg105 NE, 2.68 Å) and some different points of contact present in the WT obelin crystal. This is not the case for loop III where the closest symmetry related molecule in W92F is 6.8 Å distant and in WT more than 3.7 Å away (data not shown).

Structure of the Calcium-Binding Loops. Figure 8 shows the superimposed structures of loops III (left) and IV (right) for WT (brown) and W92F (violet) obelins. The structure of loop I is essentially the same in the two obelins (average rms deviation of the Cα and side chain atomic positions is 0.36 Å) and is therefore not shown. In canonical Ca^{2+}-binding loops the Ca^{2+} is typically coordinated in a pentagonal bipyramidal array of seven oxygen atoms belonging to residues occupying positions 1, 3, 5, 7, 9, and 12 in the loop. Residues 1, 3, and 5 provide monodentate oxygen ligands via side chain oxygens, usually aspartate carboxylates. Residue 12 is a bidentate oxygen ligand and is almost always a glutamate residue, which ligates calcium via both side chain carboxylate oxygens. Residue 7 directly coordinates Ca^{2+} via its main chain oxygen. As a rule, residue 9 hydrogen bonds to a water molecule that provides the remaining Ca^{2+} ligand. The hydrogen bond network among the loop residues has to be such that the incoming Ca^{2+} can be readily accommodated in its strictly required ligation geometry.

We have carried out thorough analysis of hydrogen bond interactions in each of the III and IV loops of WT and W92F obelins, and the results are listed in Table 2. In general the hydrogen bond networks of these Ca^{2+}-binding sites in WT and W92F obelins are very similar to each other and also similar to those of other Ca^{2+}-binding proteins (*36*). However, there are some clear differences (Table 2). Among them we want to point out Lys124 and Asp169 occupying the positions 2 of loop III and 11 of loop IV, respectively. In W92F obelin, the side chain of Lys124 is extended into the solvent as is frequently observed in other Ca^{2+}-binding proteins. But in the case of WT obelin, the N atom of the side chain of Lys124 forms a strong hydrogen bond (2.69 Å), with the O atom of the side chain of Glu134 (position 12) (Table 2) pulling together the N- and C-termini of the loop. In loop IV the side chain of Asp169 in WT obelin

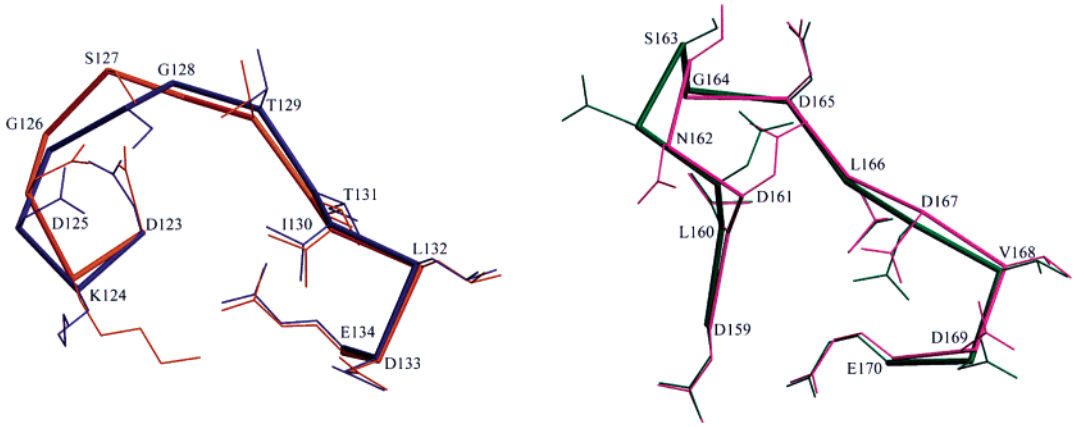

FIGURE 8: Superposition of the Ca^{2+}-binding loops III (left) and IV (right) between WT (brown) and W92F (violet) obelins. Deviations start around residues K124 and D161 in the loops of motifs III and IV, respectively.

Table 2: Putative Hydrogen Bonds within EF-Hand Loops III and IV

loop III						loop IV					
atoms				distance (Å)[a]		atoms				distance (Å)[a]	
				W92F	WT					W92F	WT
Asp123	$O^{\delta1}$	Ser127	N	3.07	3.02	Asp159	N	Glu170	$O^{\delta1}$	3.06	2.91
	$O^{\delta1}$	Gly128	N	2.80	2.84	Asp161	$O^{\delta1}$	Asn162	N	3.32	none
Lys124	N^{ζ}	Glu134	$O^{\delta1}$	none	2.69		$O^{\delta1}$	Ser163	N	2.78	2.66
Asp125	$O^{\delta1}$	Gly126	N	2.63	3.00		$O^{\delta1}$	Gly164	N	3.05	3.04
	$O^{\delta1}$	Ser127	N	2.80	2.65		$O^{\delta1}$	Asp165	N	3.04	3.06
Thr131	N	Glu134	$O^{\delta2}$	2.84	2.91		O	Gly164	N	2.91	3.20
	O	Glu134	N	3.19	3.06		N	Asp165	O	3.04	2.98
	O^{γ}	Glu134	N	3.23	3.10	Asp167	$O^{\delta1}$	Asp169	N	2.81	3.33
							$O^{\delta1}$	Glu170	N	2.73	2.93
							O	Glu170	N	3.17	3.29
							O	Met171	N	3.12	3.17

[a] The hydrogen bond distances were computed with Swiss-PDB Viewer 3.7 using constraints: maximal distance, 3.300 + 0.050 Å; minimal distance, 2.195 Å; minimal angle, 90°.

forms a strong hydrogen bond with a side chain nitrogen of Arg112 from the incoming helix of loop III, thus binding together incoming and exiting EF-hand motifs in WT obelin. However, this interaction is not present in W92F obelin. A probable consequence of these hydrogen bonds is decreased flexibility of the α-helices forming III and IV EF hands in WT obelin.

Peroxy−Coelenterazine in the Binding Site. The coelenterazine hydroperoxide is positioned in the center of the photoprotein molecule (Figure 6A). The dimensions of the binding site and the hydrogen bond interactions are nearly the same in the WT and W92F obelins (*19*), with the exception of Trp92 (Figure 9). Two water molecules (WAT) are observed to be in the same positions in WT and W92F obelins, as well as in aequorin. Despite these similarities, there are two significant differences between WT and W92F obelin.

The first and most remarkable difference has to do with the electron density around the C2 atom of coelenterazine (*19*). The density clearly corresponds to the presence of two oxygen atoms, consistent with peroxide substitution as also observed in the aequorin structure (*12*). The electron density around the second oxygen, however, is weaker than for the atoms over the rest of the coelenterazine (Figure 1), a situation also encountered for both peroxy oxygens in the aequorin structure. It is assumed that the substituent is a hydroperoxide and is stabilized by a strong hydrogen bond between the second oxygen and the hydroxyl group of Tyr190 with a distance of 2.53 Å. The hydroxyl group of Tyr190 as in WT obelin donates a hydrogen bond (2.67 Å) to the NE2 atom of His175. There is a small shift from the WT in the position of the side chain of Tyr190 (Figure 9; rms deviation 0.26 Å) but probably not so significant as to explain the appearance of the two oxygen atoms at the C2-position of coelenterazine.

We also can compare the interactions of Trp92 in WT obelin and Phe92 in W92F obelin. Both Trp92 and Phe92 form intrahelical hydrogen bonds with surrounding residues with bond lengths approximately the same in both cases. Some differences arise from the different size of the side chain. Trp92 not only forms a hydrogen bond (3.17 Å) between its NE1 nitrogen atom and the p-hydroxyphenyl group of coelenterazine, but also has multiple interactions of its side chain atoms with side chain atoms of His22, Phe88, and Tyr180 (distances all less than 3.5 Å). This combination, together with the 6-(*p*-hydroxyphenyl) group of coelenterazine, forms an aromatic cluster in this part of the coelenterazine-binding pocket, which may play some role in the function of the photoprotein. Some carbon atoms of Phe92 are at van der Waals contact, separation less than 4.18 Å, from the CE1 atom of His22.

DISCUSSION

The spatial structures of the calcium-regulated photoproteins provide some new insights into their mechanism of action and clues as to how the displacement of key residues could induce the chemical reaction of the substrate and how

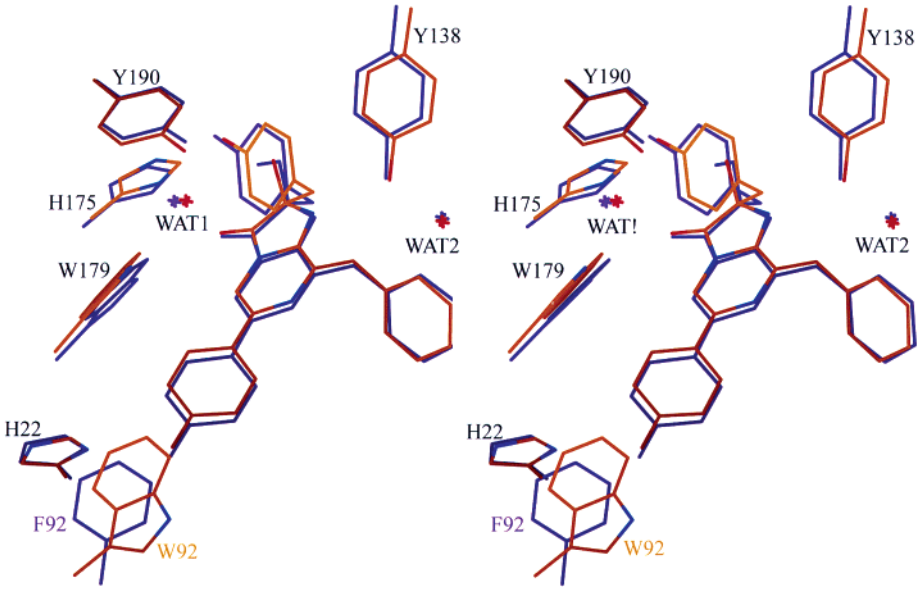

FIGURE 9: Stereo diagram showing that there is little difference in binding site structure between WT (brown) and W92F (blue) obelin.

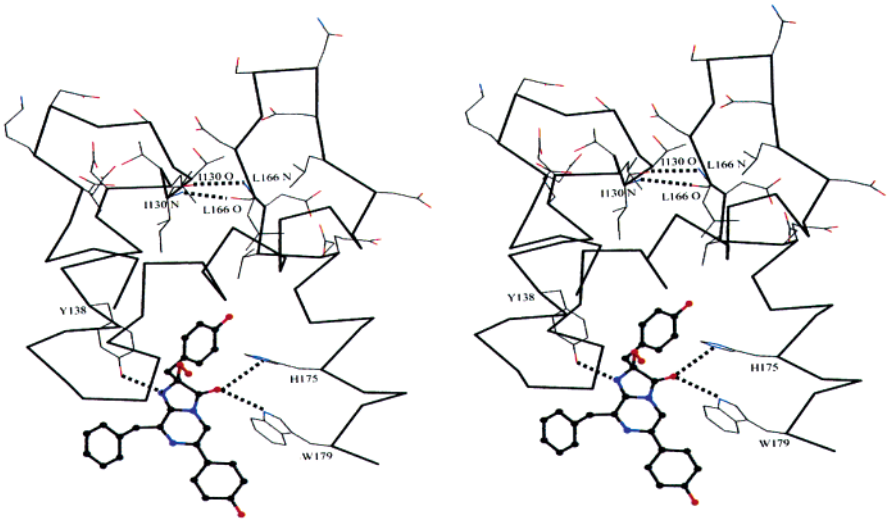

FIGURE 10: The coelenterazine binding site and nearby Ca^{2+}-binding loops of the EF-hand motifs III and IV.

different excited states of the product are populated that are responsible for the different colors of the emitted light.

Mechanism of the Bioluminescence Trigger. Certain residues within the exiting helices of loops III and IV (Figure 10), namely, Tyr138, His175, and Trp179, as well as Tyr190, have critical proximity to the substrate in the reactive center. Therefore, any conformational adjustment in the binding loops accompanying Ca^{2+} binding can be expected to propagate into shifts of the hydrogen bond donor−acceptor separations around the coelenterazine, the ones apparently essential for the hydroperoxide stability, the networks O34, Tyr190, His175, O18, and N1 to Tyr138. To initiate the shift of hydrogen donor−acceptor separations, the small spatial shift of the exiting α-helix of loop IV probably will be enough since most of the residues mentioned above are found in this α-helix. Among these residues His175 probably plays the essential role for triggering the bioluminescence reaction as in its location, it is poised to act as a general base accepting a proton from Tyr190. The enzymatic mechanism is then obvious. The p*K*'s of the Tyr hydroxyl and the hydroperoxide are very close, and any peroxy anion formed will undergo nucleophilic addition to the supposed intermediate dioxetanone, which proceeds into the decarboxylation pathway (Scheme 1). The notion that a His residue in this position is very important for photoprotein activity is supported by observations on aequorin. Site-directed mutagenesis of the five histidine residues in aequorin has shown that substitution of His169 (corresponding to His175 for obelin) with Ala, Phe, or Trp leads to almost complete loss of activity, whereas modification of the remaining four histidine residues yielded mutant aequorins with varying bioluminescence activities (*37*).

In photoproteins the first step in the generation of high-intensity bioluminescence must be the binding of Ca^{2+} to the loops within the EF hands. Comparative analysis reveals some differences between W92F and WT obelin in the structural organization of loops III and IV but not loop I (Figure 8 and Table 2). First there is deviation of atom positions of some residues, especially those, which participate directly in calcium coordination—Asp and Ser at loop positions 3 and 5. Another difference is in the hydrogen bond network, particularly the hydrogen bond between the side-chain oxygen atom of Glu134 and the side-chain nitrogen atom of Lys124, which binds together the N- and C-terminals

of the loop III in WT obelin but is not present in W92F obelin. There is also a hydrogen bond between the side-chain oxygen atom of Asp169 and the main-chain nitrogen of Arg112 which binds together the incoming α-helix of loop III and exiting α-helix of loop IV in WT, but again not present in W92F obelin. These differences in the structure of Ca^{2+}-binding loops III and IV apparently do not change the overall affinity constant to calcium of W92F obelin (Figure 4) but probably could result in changes in the speed of conformational transients that arise after binding Ca^{2+} ions. For instance, the hydrogen bond between the Arg112 main-chain nitrogen and Asp169 side-chain oxygen atoms in WT could provide the coordination of structural transients of α-helices occurring in III and IV "EF hands" after the binding of calcium ions. In W92F obelin this hydrogen bond is missing, and therefore, the exiting α-helix of loop IV in which many key residues are found, including His175, suggested by us as the crucial residue for bioluminescence reaction triggering, can have more flexibility than in WT obelin. With the caution that some of the differences in the rms deviations of the loop IV region may arise from crystal contacts as already mentioned, there remains sufficient evidence to suggest that the difference in the kinetics of the calcium-regulated bioluminescence response between WT and W92F obelins (Figure 5) could be a consequence of loop structure differences.

Evidence for a conformational change on binding Ca^{2+} in obelin has been shown by NMR (*38*). There is a clear difference in the ^{15}N-HSQC spectra between obelin and its Ca-loaded state. A structural change also occurs in aequorin following calcium addition monitored by an increase in tryptophan residue fluorescence. But the rate of this structural change is much slower than the bioluminescence emission rate (*39*), in clear support of our assumption that even a small structural adjustment could trigger the bioluminescence reaction in photoproteins.

Also, we would like to note here that the calcium-independent luminescence (*40*) that is observed for all photoproteins studied is probably just a consequence of dynamic fluctuations of the structure with a randomly small probability of altering these hydrogen bond separations. The addition of Ca^{2+} just amplifies this probability over a million times.

The Bioluminescence Emitter. Identification of the bioluminescence emitter is a key requirement in solving the reaction mechanism. In the past the approach taken has been to study the chemiluminescence reaction of the substrate or close substrate analogues, under various solution conditions that might mimic the protein reaction site environment. To qualify as the product of the light reaction, the candidate should have a fluorescence spectrum the same as the bioluminescence as well as a fluorescence quantum yield greater than the bioluminescence quantum yield. In the earliest study, McCapra and Chang (*9*) proved the mechanism of the chemiluminescence of the coelenterazine analogue in Scheme 1. In DMSO and a strong base such as potassium *tert*-butoxide, chemiluminescence of this compound occurs with a spectral emission maximum at 455 nm. The amide is produced in high yield, and under the same basic solution conditions, the fluorescence spectrum of the synthesized amide matches the chemiluminescence spectrum. The fluorescing species was identified as the excited amide anion

Scheme 3

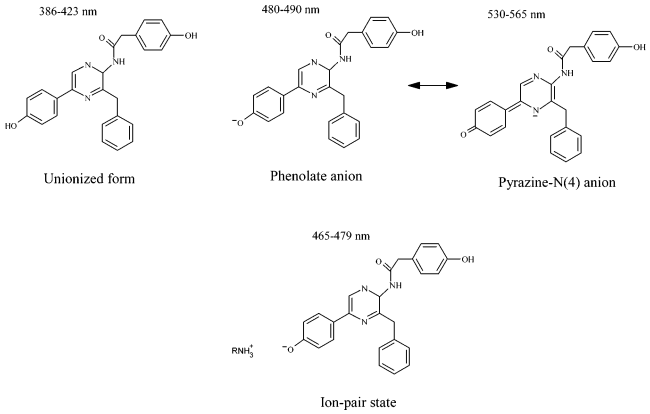

because without added base, the fluorescence maximum is at 380 nm, assigned to the neutral species.

Hori et al. (*41*) extended this Scheme 1 model with a study of the chemiluminescence properties of a number of other coelenterazine analogues, with 6-*p*-hydroxyphenyl or 6-*p*-methoxyphenyl substituents. In the aprotic solvent dimethylformamide without the inclusion of base, these compounds reacted spontaneously with dissolved oxygen to yield chemiluminescence with a spectral maximum at 480 nm. The fluorescence of the product had a spectral maximum at 402 nm the same as for the synthetic coelenteramide analogue and again attributed to the neutral form. However, when the reaction of the *p*-hydroxyphenyl analogue was made with inclusion of base, *tert*-butoxide, the chemiluminescence spectrum appeared at longer wavelength with a maximum at 535 nm, and the product fluorescence, as well as the fluorescence of the synthetic analogue of coelenteramide, was also shifted to a 535 nm maximum. Hori et al. (*41*) proposed the coelenteramide dianion, the amide anion phenolate, as the 535 nm emitting species. For the *p*-methoxyphenyl analogue, strong base produced no shift, and the chemiluminescence and fluorescence maxima remained at 480 nm. They concluded that in this case, the spectral emission was from the excited state of the amide anion.

Shimomura and Teranishi (*42*) also made an observation very relevant to the present study (Scheme 3). The fluorescence of coelenteramide in benzene has a maximum at 397 nm assigned as from the neutral excited state. However, on addition of *n*-butylamine the spectrum is bimodal with the new band maximum at 467 nm. They assigned this latter as from an ion-pair excited state. The same conclusion was reached by Imai et al. (*43*), who made a systematic study of this ion pairing of coelenteramide analogues as a function of solvent and added base. They suggested that the phenolate ion from coelenteramide had a singlet excited state with a charge-transfer character. Consequently the energy level should be very sensitive to solvent polarity. Their interpretation was that the phenolate fluorescence maximum ranged from 592 nm in aprotic polar solvents such as DMSO, to 466 nm in benzene. They concluded that the phenolate was the source of bioluminescence emission from aequorin.

Up to now, all these observations led to the generally agreed conclusion that in the bioluminescence systems involving coelenterazine, i.e., the photoproteins under consideration here and *Renilla* luciferase, as well as the related *Vargula* luciferase using a structurally similar luciferin, the

amide anion is the primary chemical product generated in its excited state from which the bioluminescence emission occurs. The range of bioluminescence spectral maxima recorded, 462 nm for the *Vargula* luciferin-luciferase reaction to 495 nm for the Ca^{2+}-triggered bioluminescence of obelin from *O. geniculata* (*23*), can be attributed to perturbation of the singlet excited-state energy level of the amide anion by the properties of the binding site environment, such as its effective dielectric constant. However, the more recent results suggest that the amide anion, the phenolate, and the neutral forms of coelenteramide are all contenders for the emitting state in the several bioluminescent reactions utilizing coelenterazine or its analogues such as the luciferin in the *Vargula* bioluminescence system.

The McCapra and Chang mechanism (Scheme 1) demands that the amide anion is the initially formed excited state and is the proven emitter of the chemiluminescence in aprotic medium. However, in bioluminescence systems the excited coelenteramide anion resides in an active site of a protein, and the attendant hydrogen bond interactions with surrounding residues allow the possibility of excited state proton transfer changing the nature of the emitting state. Such processes are known to be fast, on the nanosecond timescale and therefore highly competitive with the radiative rate of the amide anion.

Without knowledge of the calcium triggered protein structure but taking into account that gross conformation changes are much slower than the bioluminescence emission rate as was demonstrated for aequorin (*39*), we will assume for discussion that the configuration of the coelenterazine binding site is almost unchanged in the time span for generating the excited coelenteramide. The first proton transfer that can be expected is to form the excited neutral species. An amide group is only dissociable in an aprotic solvent under very basic conditions, and although it is known that the excited state p*K* could be lowered over the ground state, there are a number of proton sources in the binding site (Figure 10) that would favor rapid formation of the neutral excited state. The second target for proton transfer is at the 6-p-hydroxyphenyl position of the coelenterazine. In WT obelin, this hydroxy group is hydrogen bonded to His22 and Trp92 (Figure 10). As the excited state p*K* of this group is likely to be substantially lowered from the ground-state value, a complete proton transfer to His22 is feasible, producing the ion-pair excited state. Thus, the possibility of proton transfer at these two positions around coelenteramide could result in a mixture of neutral and ion-pair excited states and in fact, the bioluminescence emissions from the obelins (*23*) as well as the *Renilla* luciferase reaction (*44*), all show a small contribution from a 400 nm band on the major band around 480 nm. The cited model fluorescence studies assign the 480 nm band as from a coelenteramide ion-pair excited state (*42*) and 400 nm from the neutral species. The deuterium effect on the relative population of the excited-state species (Figure 3, *right*) gives additional support to these excited state proton transfer ideas. In conclusion, we propose that the bioluminescence of WT obelin originates from the coelenteramide phenolate ion-pair excited state with a small admixture of the neutral excited state, both rapidly formed from the primary excited amide anion.

As a matter of record, Shimomura et al. (*39*, *45*) were the first to observe a bimodal bioluminescence spectrum from what they called *e*-aequorin, an artificial photoprotein formed by charging the apoaequorin with a coelenterazine analogue containing an extra ethano bridge. Ohmiya et al. (*17*) produced the aequorin mutant W86F, which showed an enhanced 405 nm contribution just using coelenterazine but this 405 nm band became dominant if the fused ring analogue was employed. Without structural information it is impossible to know what is going on with the analogues but a steric effect is likely, where the fused ring structure alters the separation of the *p*-hydroxyl group and the His16 in the case of aequorin. The contribution of the 405 nm emission originating from the excited state of the neutral coelenteramide in the corresponding mutant of obelin, W92F, is even greater than that in W86F aequorin (*19*). The idea of dual proton transfer after primary excited amide anion formation and of the 480 nm bioluminescence originating from the excited phenolate in an ion-pair interaction with the His22 also allows other observations to fall into place. At a pH below 7, the His22 is protonated and can no longer accept a proton to form the excited phenolate in competition with the radiative rate from the neutral excited coelenteramide (Figure 3, left). Hydrogen bonding from the Trp92 in WT obelin could stabilize the ion-pair state favoring longer wavelength emission, and that is why its removal produces the violet bioluminescence and the bimodal emission spectrum. We need to caution here that it is not possible to exclude that this substitution could change dielectric properties of the environment of the p-hydroxyl group. As a result the relevant p*K*'s could be changed with resulting influence on the proton-transfer rate from p-hydroxyl group to His22.

Why the aequorin bioluminescence maximum at 465 nm (*46*) is different from those of the obelins, 485 and 495 nm (*23*), is not clear, as the residues in the binding site and its dimensions in the two proteins are almost the same. The answer could be in small variation of hydrogen bond distances between coelenterazine and key residues in these photoproteins (*12*, *13*) that can influence proton transfer rates of the excited coelenteramide, and in the structure of the cavity enclosing the excited coelenteramide immediately following the bioluminescence triggering that can provide both an appearance of new hydrogen bonds with excited coelenteramide and a change of polarity of the environment. For instance, in aequorin the product fluorescence spectral distribution is the same as the bioluminescence (*46*), but the obelin product fluorescence is shifted 25 nm to longer wavelength than its bioluminescence (*23*). NMR evidence shows that there is a conformation change appearing after the calcium-induced bioluminescence of obelin (*38*), so if the binding site becomes more exposed to solvent—that is, polar—then shifts to longer wavelength would result. The obelin product fluorescence spectrum matches the coelenteramide phenolate spectrum in more polar solvents (*42*). Removal of the calcium causes a further conformation rearrangement as observed by NMR (*38*), and there is also a small change in fluorescence and absorption spectra as well. These data, together with coelenteramide fluorescence studies (*42*, *43*), clearly indicate that polarity has strong influence on emission spectrum. Therefore, even small conformational changes and resulting changes in equivalent dielectric constant of the binding site could easily be sufficient to account for the differences in bioluminescence spectra among the photoproteins and also for the differences of the obelin

bioluminescence spectra and the fluorescence of the product.

Application of W92F Obelin to Intracellular Calcium Assay. Photoproteins have been used successfully in a great many different types of living cells both to estimate the intracellular [Ca^{2+}] under steady-state conditions and to study the role of calcium transients in the regulation of cellular function. W92F obelin is the fastest responding among investigated calcium-regulated photoproteins, several times faster, for example, than the commonly used aequorin. Some other characteristics of W92F obelin—sensitivity to calcium, specific activity, calcium-independent bioluminescence, temperature stability, coelenterazine binding kinetics—are practically unchanged from the WT obelin.

In addition to faster kinetics of bioluminescence response, there is another very attractive prospect for application of this mutant. Because the bioluminescence from W92F obelin is violet (λ_{max} = 405 nm) rather than the blue for the WT obelin (λ_{max} = 485 nm), synchronous measurements of intracellular calcium transients in different compartments of the cell is an interesting possibility. This would be achieved through simultaneous expression of DNAs encoding W92F obelin and WT obelin with different target sequences directing these photoproteins into different compartments of the cell. Even without additional improvement of spectral characteristics, distinguishing the two emission spectra is quite feasible using narrow bandwidth transmission filters. This approach could allow estimation of coupled transients of intracellular calcium in different cell compartments, potentially leading to an improved understanding of the regulator function of calcium ions for various cell processes.

REFERENCES

1. Bondar, V. S., Trofimov, K. P., and Vysotski, E. S. (1992) *Biochemystry (Moscow) 57*, 1020−1027 (in Russian).
2. Illarionov, B. A., Bondar, V. S., Illarionova, V. A., and Vysotski, E. S. (1995). *Gene 153*, 273−274.
3. Morin, J. G. (1974) in *Coelenterate Biology: Reviews and New Perspectives* (Muscatine, L., and Lenhoff, H. M., Eds.) pp 397−438, Academic Press, New York.
4. Shimomura, O., Johnson, F. H., and Saiga, Y. (1962) *J. Cell. Comp. Physiol. 59*, 223−239.
5. Charbonneau, H., Walsh, K. A., McCann, R. O., Prendergast, F. G., Cormier, M. J., and Vanaman, T. C. (1985) *Biochemistry 24*, 6762−6771.
6. Tsuji, F. I., Ohmiya, Y., Fagan, T. F., Toh, H., and Inouye, S. (1995) *Photochem. Photobiol. 62*, 657−661.
7. Moncrief, N. D., Kretsinger, R. H, and Goodman, M. (1990) *J. Mol. Evol. 30*, 522−562.
8. Nelson, M. R., and Chazin, W. J. (1998) *BioMetals 11*, 297−318.
9. McCapra, F., and Chang, Y. C. (1967) *Chem. Commun. 19*, 1011−1012.
10. Morin, J. G., and Hastings, J. W. (1971) *J. Cell. Physiol. 77*, 305−311.
11. Shimomura, O., and Johnson, F. H. (1978) *Proc. Natl. Acad. Sci. U.S.A. 75*, 2611−2615.
12. Head, J. F., Inouye, S., Teranishi, K., and Shimomura, O. (2000) *Nature 405*, 372−376.
13. Liu, Z.-J., Vysotski, E. S., Chen, C. J., Rose, J. P., Lee, J., and Wang, B.-C. (2000) *Protein Sci. 9*, 2085−2093.
14. Vysotski, E. S., Liu, Z.-J., Rose, J., Wang, B.-C., and Lee, J. (2001) *Acta Crystallogr., Sect. D: Biol. Crystallogr. 57*, 1919−1921.
15. Liu, Z.-J., Vysotski, E., Deng, L., Lee, J., Rose, J., and Wang, B.-C. (2002) *Luminescence 17*, 99.
16. Kawasaki, H., Nakayama, S., and Kretsinger, R. H. (1998) *Biometals 11*, 277−295.
17. Ohmiya, Y., Ohashi, M., and Tsuji, F. I. (1992) *FEBS Lett. 301*, 197−201.
18. Hori, K., Wampler, J. E., Matthews, J. C., and Cormier, M. J. (1973) *Biochemistry 12*, 4463−4468.
19. Deng, L., Vysotski, E. S., Liu, Z.-J., Markova, S. V., Malikova, N. P., Lee, J., Rose, J., and Wang, B.-C. (2001) *FEBS Lett. 506*, 281−285.
20. Hastings, J. W., Mitchell, G., Mattingly, P. H., Blinks, J. R., and Van Leeuwen, M. (1969) *Nature 222*, 1047−1050.
21. Markova, S. V., Vysotski, E. S., and Lee, J. (2001) in *Bioluminescence & Chemiluminescence 2000* (Case, J. F., Herring, P. J., Robison, B. H., Haddock, S. H. D., Kricka, L. J., and Stanley, P. E., Eds.) pp 115−118. World Scientific Publishing Company, Singapore.
22. Illarionov, B. A., Frank, L. A., Illarionova, V. A., Bondar, V. S., Vysotski, E. S., and Blinks, J. R. (2000) *Methods Enzymol. 305*, 223−249.
23. Markova, S. V., Vysotski, E. S., Blinks, J. R., Burakova, L. P., Wang, B.-C., and Lee, J. (2002) *Biochemistry 41*, 2227−2236.
24. Vysotski, E. S., Liu, Z.-J., Rose, J., Wang, B.-C., and Lee, J. (1999) *Acta Crystallogr., Sect. D: Biol. Crystallogr. 55*, 1965−1966.
25. Otwinowski, Z., and Minor, W. (1997) *Methods Enzymol. 276*, 307−326.
26. Jones, T. A., Zou, J. Y., Cowan, S. W., and Kjeldgaard, M. (1991) *Acta Crystallogr., Sect. A 47*, 110−119.
27. Brunger, A. T., Adams, P. D., Clore, G. M., DeLano, W. L., Gross, P., Grosse-Kunstleve, R. W., Jiang, J. S., Kuszewski, J., Nilges, M., Pannu, N. S., Read, R. J., Rice, L. M., Simonson, T., and Warren, G. L. (1998) *Acta Crystallogr., Sect. D: Biol. Crystallogr. 54*, 905−921.
28. Laskowski, R. A., MacArthur, M. W., Moss, D. S., and Thornton, J. M. (1993) *J. Appl. Crystallogr. 26*, 283−291.
29. Luzatti, V. (1952) *Acta Crystallogr. 5*, 802−810.
30. Blinks, J. R., Mattingly, P. H., Jewell, B. R., van Leeuwen, M., Harrer, G. C., and Allen, D. G. (1978) *Methods Enzymol. 57*, 292−328.
31. Klabusay, M., and Blinks, J. R. (1996) *Cell Calcium 20*, 227−234.
32. Blinks, J. R., and Moore, E. D. W. (1986) in *Optical Methods in Cell Physiology* (De Weer, P., and Salzberg, B. M., Eds.) Vol. 40, pp 229−238. John Wiley, New York.
33. Gibson, Q. H., and Milnes, L. (1964) *Biochem. J. 91*, 161−171.
34. Kurose, K., Inouye, S., Sakaki, Y., and Tsuji, F. I. (1989) *Proc. Natl. Acad. Sci. U.S.A. 86*, 80−84.
35. Bondar, V. S., Frank, L. A., Malikova, N. P., Inzhevatkin, E. V., Illarionova, V. A., and Vysotski, E. S. (1999) in *Bioluminescence & Chemiluminescence: Perspectives for the 21st Century* (Roda, A., Pazzagli, M., Kricka, L. J., and Stanley, P. E., Eds.) pp 400−403, John Wiley & Sons, Chichester.
36. Strynadka, N. C. J., Cherny, M., Sielecki, A. R., Li, M. X., Smillie, L. B., and James, M. N. G. (1997) *J. Mol. Biol. 273*, 238−255.
37. Ohmiya, Y., and Tsuji, F. I. (1993) *FEBS Lett. 320*, 267−270.
38. Lee, J., Glushka, J. N., Markova, S. V., and Vysotski, E. S. (2001) in *Bioluminescence & Chemiluminescence 2000* (Case, J. F., Herring, P. J., Robison, B. H., Haddock, S. H. D., Kricka, L. J., and Stanley, P. E., Eds.) pp 99−102, World Scientific Publishing Company, Singapore.
39. Shimomura, O. (1995) *Biochem. J. 306*, 537−543.
40. Allen, D. G., Blinks, J. R., and Prendergast, F. G. (1977) *Science 195*, 996−998.
41. Hori, K., Wampler, J. E., Matthews, J. C., and Cormier, M. J. (1973) *Biochemistry 12*, 4463−4468.
42. Shimomura, O., and Teranishi, K. (2000) *Luminescence 15*, 51−58.
43. Imai, Y., Shibata, T., Maki, S., Niwa, H., Ohashi, M., and Hirano, T. (2001) *Photochem. Photobiol. A: Chemistry 146*, 95−107.
44. Hori, K., Charbonneau, H., Hart, R. C., and Cormier, M. J. (1977) *Proc. Natl. Acad. Sci. U.S.A. 74*, 4285−4287.
45. Shimomura, O., Musicki, B., and Kishi, Y. (1988) *Biochem. J. 251*, 405−410.
46. Shimomura, O., and Johnson, F. H. (1970) *Nature 227*, 1356−1357.

BI027258H